Study of the particle motion induced by a vortex shaker

Somik Chakravarty, Marc Fischer, Pablo García-Tríñanes, David Parker, Olivier Le Bihan, Martin Morgeneyer

PII: S0032-5910(17)30672-1
DOI: doi: 10.1016/j.powtec.2017.08.026
Reference: PTEC 12765

To appear in: *Powder Technology*

Received date: 2 June 2017
Revised date: 2 August 2017
Accepted date: 6 August 2017

Please cite this article as: Somik Chakravarty, Marc Fischer, Pablo García-Tríñanes, David Parker, Olivier Le Bihan, Martin Morgeneyer, Study of the particle motion induced by a vortex shaker, *Powder Technology* (2017), doi: 10.1016/j.powtec.2017.08.026

Study of the particle motion induced by a vortex shaker

Somik Chakravarty[1,*], Marc Fischer[a,b], Pablo García-Tríñanes[c], David Parker[d], Olivier Le Bihan[b], Martin Morgeneyer[a]

[a] *Université de Technologie de Compiègne (UTC) Sorbonne Universités, Laboratoire Transformations intégrées de la matière renouvelable (TIMR), Rue Roger Couttolenc, CS 60319, 60203 Compiègne Cedex, France*
[b] *Institut National de l EnviRonnement Industriel et des RisqueS (INERIS), NOVA/CARA/DRC/INERIS, Parc Technologique Alata, BP2, F-60550 Verneuil-En-Halatte, France*
[c] *Wolfson Centre for Bulk Solids Handling Technology, University of Greenwich, London, United Kingdom*
[d] *School of Physics and Astronomy, University of Birmingham, Birmingham, United Kingdom*

Keywords:
PEPT Powder Vortex-shaker Dustiness

Abstract The behaviour of a traced alumina particle lying on limestone powders with similar features has been studied in a test tube agitated by a vortex shaker aiming at studying dust emissions from powders. PEPT (Positron Emission Particle Tracking) was used for measuring the particle's position. Population densities were computed as the frequency of the particle's presence in different regions dividing the two horizontal axes and the vertical axis, respectively. The velocities of the particle were calculated by filtering out all displacements inferior to a critical distance d_{crit} so as not to consider spurious movements caused by experimental noise. After its validation, the methodology was applied to the standard condition of a vortex shaker experiment ($\omega = 1500$ rpm, 2 g of powder and open test tube). While the horizontal coordinates and velocity components follow a symetric distribution, the vertical coordinate is characterised by a large asymetrical plateau. The heights reached by the particle (up to 24.3 mm) are small in comparison to that of the test tube (150 mm). The greatest velocities are found near the inner wall of the test tube and at the highest heights where the population densities are the lowest. The median velocity of the particle is 0.0613 m.s^{-1} whereas its median kinetic energy is 8.4E-12 J. The method explicated in the present study is directly applicable to any other sets of data obtained through PEPT, especially if the system is of small dimension.

1. Introduction

One necessary condition for reaching a better theoretical understanding of dust emission in a tester is a good understanding of the detached particle's motion within the system. This prompted us to undertake the present work where the motion of a single particle has been followed in a test tube agitated by a vortex shaker for several hundreds of seconds. Dust aerosols are small solid particles, conventionally taken as those particles below 75 μm in diameter,

*Corresponding author: somik.chakravarty@utc.fr

which settle out under their own weight but which may remain suspended for some time, according to the International Standardisation Organization (ISO 4225 - ISO, 1994) [1]. The tendency of materials to form aerosols upon handling is known as their dustiness [2, 3]. Dustiness studies are important for analysing the industrial risks posed by a bulk material in terms of worker exposure to particles by inhalation, contamination of products and equipments, loss of material and release to the environment [4].

The dustiness of a material is not only related to its physical parameters but also depends on the nature and intensity of the stresses exerted on it alongside external conditions such as humidity and ventilation [2, 5]. The tendency of a material to generate dust under certain conditions can be evaluated using meso-scale lab testers [6, 7]. For a specific amount of powder, they provide energy to the system for a given period of time. The amount of energy is ideally selected in such a way that it is enough to overcome the adhesive forces between the particles of the bulk solids, thereby emitting dust particles in the air beyond the threshold of measurability. The aerosol concentration and the particle size distribution are then measured as a function of time. Although the dustiness testers are generally designed in such a way that the input energy and dust generation mechanisms are close to industrial situations [8, 9], there are only few studies which directly compare the experimental and industrial conditions [10]. This limits our ability to understand, simulate and predict dustiness under industrially relevant circumstances [11]. There exists a wide range of such testers which have been reviewed by several authors [12–14], yet no universal dustiness testing method delivering consistent results under all circumstances could be developed [13]. The European standard 15051 on the *Measurement of dustiness of bulk material* [15] mentions the continuous drop tester and the rotating drum method but their applicability to the test of mico- and nano-scale powders has been limited as they require large amounts of powder (35cm^3 or 500g), thus increasing the experimental cost and also the risk of exposure to aerosol particles of the persons conducting the test [16].

The *vortex shaker* (VS) [17, 18] (or vortex mixer) enables the measure of dustiness with only a fraction (2 g) of the powder which would have been required by other standardised testers. The system is relatively cheap and easy to operate. It seems to be a promising approach to measuring the dustiness of fine cohesive powders [8]. Aerosols are generated through the agitation of a powder-filled symmetrical cylindrical test tube mounted on a digital vortex shaker capable of achieving rotation speeds along the vertical axis. There have been several studies looking into the effect of the VS speed and sample mass on the aerosol concentration (expressed with respect to their masses and numbers) [3, 6, 17]. However, to the best of our knowledge there has not been any study investigating the effect of

the rotational agitation on the powder particle *motion*.

While there are optical methods, such as the laser Doppler anemometer (LDA) [19] and the particle image velocimetry (PIV) [20], for studying the average velocity fields in a range of flow systems [21–23], they are not well suited for opaque systems [24, 25] and consider generally rather low concentrations of particles in the fluid phase [26, 27]. Our own approach consists of the Langrangian tracking of an individual particle [28, 29] placed in the powder bed of the test tube which is then agitated by the vortex shaker. The cyclical trajectory of the particle measured at a high frequency over a large duration provides us with *statistical information* about the behaviour of a powder primary particle detached from the bulk.

We use the Positron Emission Particle Tracking (PEPT) method for tracking a single radioactive tracer particle. It is a non-invasive study of the motion of a particle representative of the other detached powder particles subjected to the same stress conditions. A PEPT analysis of a particle's trajectory over a wide interval (largely superior to one period) can provide us with valuable statistical information such as population densities, velocities or kinetic energies. These, in turn, would provide us with the first experimental data that can subsequently be used for the validation of CFD (Computationally Fluid Dynamics) and DE (Discrete Elements) models. Such studies would prove very valuable for assessing the frequency and effects of particle-particle and particle-wall interactions.

The goal of our work are to establish a well-founded methodology for studying the traced particle's behaviour within the agitated test tube and then to apply it to the standard case of the vortex shaker induced agitation (1,500 rpm) with a vertical gaseous flow of 0.7 $\mathrm{L.min^{-1}}$ going through the agitated test tube filled with 2 g of powder.

In Section 2, we go into the technique of PEPT, and its application to the vortex shaker experimental setup. In Section 3, we present and validate the statistical strategy we use to determine the particle's position, velocity and kinetic energy. In Section 4, we apply our methodology to the particle's movement in our reference case ($\omega = 1500$ rpm, open test tube, 2 g of powder). Finally, in Section 5, conclusions are drawn and an outlook for future studies is given.

2. Experimental foundations

2.1. Vortex shaker dustiness tester

The use of a vortex shaker as a method for generating dust particles from powders is a relatively new and promising technique which has the advantage of being able to use very small quantities of powder [8, 17]. This makes the vortex

shaker method a practical and inexpensive dustiness tester when compared to the standardised dustiness testers including the rotating drum and the drop-test. A vortex shaker can be seen in Figure 1. The vortex shaker method used for this study consists of a digital vortex shaker (VWR Signature Digital Vortex Mixer, USA). Such shakers or mixers are commonly used in laboratories to mix small quantities of liquids. It consists of an electric motor with a drive shaft oriented vertically, which is connected to a rubber cup mounted slightly off-center. Dust is generated from a small amount (around 2 g) of bulk solid sample contained in a glass centrifuge tube (diameter 0.025 m, height 0.150 m) firmly mounted on the rubber cup. As the motor runs, the rubber cup oscillates rapidly in a circular motion and the motion is transmitted to the solid sample inside the cylindrical tube. The shaker is capable of generating a uniform vortex action with rotational velocities ranging between 500 rpm and 2,500 rpm along the vertical axis.

Due to the centrifugal forces generated in the vortex shaker setup, the particles in the bulk sample can be assumed to undergo the outward centrifugal force acting as a separation force, the vertical gravitational force and attractive surface forces between the particles acting as binding forces. This phenomenon can be qualitatively seen after each vortex shaker experiment where the bulk sample generates a hollow center whereas the particles accumulate towards the wall and can also adhere to the wall surface (as shown in the appendix, see Fig. A.1).

2.2. PEPT and the tracer particle

Positron emission particle tracking (PEPT) is an experimental technique allowing one to follow the movements of a radioactive tracer particle [30]. This method has been adapted from Positron Emission Tomography (PET) and it is used in particle technology for studying the dynamic behaviour of dry particulate systems such as gas-fluidised beds, tumbling mills, pneumatic conveying etc. used in various industrial processes [31–34]. PEPT allows for non-invasive particle imaging and tracking deep within the particulate system for an extended period of time, thus enabling the analysis of the in-situ kinematics and dynamics of the particle flow [35, 36]. We briefly describe the use of a tracer particle in the PEPT technique. For more detailed descriptions of the technique, we refer the interested reader to the following works [34, 37–39]. A scanning device detects the positrons (sub-atomic particles) emitted by a single tracer particle coated (labelled) with the radionuclide. The tracer particle labelled with a positron emitter ^{18}F [40] with a half-life of 109 minutes decays via β^+ decay, resulting in two gamma rays, each of which travelling in exactly opposite directions with an energy of 511 keV . The simultaneous detection of the two gamma rays in an array of detectors (using a positron camera) defines a line along which the annihilation of positrons with electrons occurs. The detection of many such events in a short time interval of approximately 10 ms allows the position of the tracer particle to be

triangulated in three dimensions. This, in turn, makes the analysis of the trajectory of the tracer particle possible. The spatial location of the tracer particle may be achieved at a frequency reaching values as high as 250 Hz with an accuracy which depends on the speed and activity of the tracer particle. Using an ADAC Forte positron camera [41] installed at the Positron Imaging Centre at the University of Birmingham, a tracer particle moving at 1 m/s can be located within 0.5 mm of its actual position, 250 times per second. To capture the dynamic behavior of the system, the tracer particle used for a PEPT study should ideally be identical or very similar with respect to its physical characteristics to the bulk material used in the system [42, 43].

Also, the radioactivity of the tracer should be high enough (preferably 300 1000 μCi) for uninterrupted tracking of the particle [44]. Thus, PEPT allows for the analysis of the motion of the particle in a complex physical system such as the vortex shaker, where it is influenced by a combination of forces including the centrifugal forces, vibration and particle-particle and particle-wall interactions. In addition to that, it can be used to determine the density of particles at each point of the setup, under the assumption that the behaviour of the traced particle over a large time period is a good approximation of the average behaviour of the ensemble of detached particles.

2.3. Test protocol

The experiments were performed at the Positron Imaging Centre, Nuclear Physics research group, University of Birmingham. A detailed description of the PEPT is mentioned in [34, 37, 45] and here we mention only the procedures related to the vortex shaker dustiness tester.

We took 2 g of Eskal 150 calcium carbonate powder weighed with an accuracy of $\pm$ 0.01 g using an analytical balance (Mettler Toledo MS104TS), manually filled in the centrifuge tube (diameter 0.025 m, height 0.15 m). The size distribution of the primary particles is such that the median diameter is 138 μm , d_{10} = 97 μm and d_{90} = 194 μm (see [46]). The diameter of the tracer particle has been chosen in such a way to be between 80 m and 150 m. The density is 2710 kg.m^{-3}.

We first labelled such a $CaCO_3$ particle using ^{18}F radionuclide (whose half-life is 109 min). However, due to the poor activation and insufficient radioactivity of the Eskal limestone particles, the calcium carbonate tracer particle was replaced by a gamma-alumina particle which showed sufficient radioactivity for more than few hours after the activation. The ^{18}F radionuclide in the tracer particle exists as structural elements about 0.3 mm under the tracer surface and is most likely unaffected by the existing ions or worn out during the test [44]. The used gamma-alumina particles from Alfa Aesar, USA had diameters between 80μm and 150μm with a purity of 99.9% and a particle density

of 2950 kg.m^{-3} similar to the features of the Eskal 150 powder used as the bulk powder during the vortex shaker experiment.

For the experiments, the powder-filled centrifuge tube was sealed using a rubber stopper (0.02 m in depth) with an opening for the inlet and outlet using two stainless steel pipes (inner diameter, 0.003 m) placed beyond 30 mm inside the tube opening piercing through the rubber stopper. The air was sucked in by a low-pressure pump (0.7 $\pm$ 0.01 L.min^{-1} or 1e-05 $\pm$ 1.6e-07 m^3.s^{-1}, Gilian LFS-113DC). The tracer particle was prepared using an indirect (water based) radioactive labelling technique in contrast to the direct bombardment of the particle itself. A heat lamp assisted then the evaporation of the radioactive water. The particle tracer was then manually transferred from its holder to a powder-filled centrifuge tube, which was mounted on the vortex shaker system placed between the positron camera (detectors). The transfer of the tracer particle into the tube and its presence in the test tube through the test duration was ensured using a Geiger counter. The vortex shaker was rotated at 1,500 rpm and run for 12 minutes. The trial was repeated once. The powder bed covered a height of 6 mm lying on the round bottom of the test tube. It was not possible to determine the initial position of the traced particle.

3. Presentation of the statistical methodology

This section aims at defining and illustrating a sound methodology suitable for studying the movement of the particle inside the agitated test tube.

3.1. Raw data and measurement uncertainties

The raw data come in the form of *relative* coordinates of the traced particle measured in very short time intervals (of roughly 10 ms). The position of the test tube with respect to the detectors may change from trial to trial because of its being mounted and unmounted. As a consequence, only the relative movements of the particle can be seen. Therefore, we defined the coordinate system as follows. We defined the height in such a way that $y = 0$ corresponds to the lowest position of the particle which has ever been measured during the trial under consideration. We defined the horizontal coordinates x and z in such a way that $x = 0$ and $z = 0$ become the *median* position which are stabler statistical indicators than the means [47]. Given the symetrical nature of the system, this proved a good strategy. We show the three axes within the test tube in Figure 2. The PEPT data are given in a cartesian frame and can thus be more readily interpreted in that way. Researchers interested in cylindrical coordinates could easily transform our results into that system of representation.

In order to compute velocities and other quantities based on the raw data, it is necessary to make a distinction between random experimental uncertainties and fluctuations of the position stemming from turbulence or other physical phenomena. For that sake, a trial where the particle position was tracked in a non-agitated and closed test tube (i.e. $\omega = 0$ rpm) has been considered. If the diffusion of particles whose aerodynamic diameters are higher than 50 μm can be neglected, random errors should be the only cause of any observed change. In Figure 3, the "position" (x, y, z) is represented as a function of time. It can be clearly seen that the measurement uncertainties cause rapid chaotic oscillations of the values which cannot be attributed to the physical state of the system. As a consequence, it is not possible to define velocities *locally* as this could artificially attribute a highly fluctuating speed to an immobile particle. In Figure 4, the averaged coordinates of the particle are given for different numbers of time points utilised to compute the local means (e.g. around $t = 300.0$ s). Even if relatively large numbers of time points are considered to calculate the mean values, the quantities are not constant, which means that the experimental noise is not erased. What is more, we noticed that averaging over more than 30 points may hide many of the physical trends observed during non-stationary trials. Consequently, another approach was adopted.

3.2. Definition of the strategy

These considerations led us to devise the following strategy for studying the particle's behaviour in the test tube.

- Only the *steady state* of the experiment is considered. It is the time period after the transition following the starting of the vortex shaker and before the device is switched off. It was determined in each case by analysing the raw data (x,y,z) as a function of time.

- The frequency of the particle being at the position x, y or z is estimated as the number of times its position belongs to the interval $[x \pm \Delta_x]$, $[y \pm \Delta_y]$ or $[z \pm \Delta_z]$, respectively. Since the measurement errors follow more or less a random distribution (see appendix, Fig. A.3), they can be expected to cancel out while considering the large samples we have at our disposal.

- Every time the particle displays a change in position equal to or greater than a critical distance (i.e. $d \geq d_{crit}$), a velocity is defined as the ratio of d and the time Δt corresponding to the displacement. The value of the critical distance d_{crit} must be chosen in such a way that ideally as few spurious coordinate fluctuations as possible are considered while the real physical movements of the particle are captured. Such a trade-off requires a process of trials and errors. The trajectory is filtered in such a way that the displacement from a point P_1 to a point P_2 is

only considered as a genuine movement if the covered distance d is greater than or equal to d_{crit}.

- Frequency distributions of the values of the above velocities and kinetic energies are computed.
- The *locally averaged* velocities $\bar{V}$, $\bar{V_x}$ (horizontal motion) and $\bar{V_y}$ (vertical motion) have been expressed as a function of x and y.

3.3. Analysis of the strategy

We then analysed the consistency of our filtering approach, partially relying on the data considered in Section 4.

The first step was to check that the filtered velocity defined above corresponds to genuine trajectories. Ideally, the measurement errors should be filtered out without overlooking important features of the traced particle trajectory. In Figure 5, the vectors corresponding to the pseudo-trajectory under stationary conditions (i.e. closed test tube, $\omega =$ 0 rpm) have been represented before and after the filtering in the (x,y) plane. It can be seen that the measurement errors are randomly distributed and do not show any consistent trajectory. The artificial displacement vectors are erased upon filtering.

It is worth noting that authors such as [34] used averaging over a relatively long period of time (e.g 10 s) to carry out their analyses. Such an approach would not work in our case as the particle can considerably change its direction (up to ten times) within only 2 s. Averaging would thus lead us to unphysical velocities which do not correspond to the real movements of the particle. [33] utilised an alternative approach consisting of smoothing the velocity using a given number of neighbouring points. In the case of 10 neighbouring points, the velocity with respect to the coordinate i is defined as follows:

$$\begin{aligned} u_{p,i}(t_k) = 0.1\left(\frac{P_{k+5,i}-P_{k,i}}{t_{k+5}-t_k}\right) + 0.15\left(\frac{P_{k+4,i}-P_{k-1,i}}{t_{k+4}-t_{k-1}}\right) \\ +0.25\left(\frac{P_{k+3,i}-P_{k-2,i}}{t_{k+3}-t_{k-2}}\right) + 0.25\left(\frac{P_{k+2,i}-P_{k-3,i}}{t_{k+2}-t_{k-3}}\right) \\ +0.1\left(\frac{P_{k+1,i}-P_{k-4,i}}{t_{k+1}-t_{k-5}}\right) + 0.15\left(\frac{P_{k,i}-P_{k-5,i}}{t_k-t_{k-5}}\right) \end{aligned}$$

The points directly surrounding k receive a weight of 0.5 whereas the most distant ones receive the smallest coefficients.

In Figure 6, the filtered and smoothed trajectory during one trial at $\omega = 1500$ rpm in a test tube with inlet and outlet flow have been represented for a duration of 2 s. One can recognise that the main trends of the trajectory are well represented by the filtered vector field. Thus, our filtering appears to be a good compromise for removing most

random experimental errors without losing track of the genuine movements of the particle. The optimal value used for obtaining these curves proved to be $d_{crit} = 5$ mm. The interpolated velocity has been systematically multiplied by the difference in time Δt between two points of the filtered trajectory. In this way, the magnitude of the motion can be compared as well. It can be seen that both the directions and values of the smoothed velocity can differ significantly from those of the filtered one. No improvement could be achieved for other numbers of neighbouring points.

We also applied filtering and smoothing to a perfectly circular movement of radius 12.5 cm taking place for 1 s, which is the duration of a *real* circular movement happening between $t = 100.30$ s and $t = 101.30$ encompassing 76 points. The results are shown in Figure 7. Whilst the filtered velocities correspond to real distances covered by the particle, there is a priori *no guarantee* that the smoothed velocities are a good approximation to the particle's real behaviour, regardless of the number of neighbouring points. The same can be said about the averaging over 20 points, despite the fact that such a number is not large enough to even out the experimental noise, as can be seen in Figure 4. All these difficulties led us to consider filtering as a straightforward and easily implementable approach for estimating the velocity distribution of the traced particle.

As can be seen in Section 4 and in the appendix (see Figures A.4 - A.8), the population densities (frequencies of presence) computed using all unfiltered points during the steady state and the frequencies of the velocity and the kinetic energy values based on the filtered trajectory are coherent and similar for two repeteaded trials.

4. Analysis of the particle's behaviour under standard conditions

The population densities and frequency distributions of the velocity and kinetic energy were considered to assess the movement of the particle under standard conditions (open test tube, $\omega = 1500$ rpm and 2 g of powder). For that sake, the two repeated trials were taken into consideration. We refer the reader to the appendix for seeing graphics systematically comparing the two repeated trials for every variable (see Figures A.4 - A.8). In what follows, we only show the first trial in the graphics. Q_1 and Q_2 are the first and second quartile, respectively. Along with the median, they are robust statistical indicators of trends in a series of data [47]. The frequency distribution of the coordinates and velocity components are shown in Figure 8 whereas the corresponding statistical indicators are given in Table 1 and 2.

Table 1: Statistics related to the movement

Trial	Min	Max	Q_1	Median	Q_2	Std Dev
			x (mm)			
1	-10.90	10.90	-3.50	0.00	3.50	4.68
2	-11.01	11.00	-3.31	0.00	3.10	4.61
			z (mm)			
1	-12.80	11.80	-3.40	0.00	3.40	4.48
2	-11.50	12.21	-3.30	0.00	3.00	4.38
			y (mm)			
1	0.00	23.80	6.60	11.01	15.60	5.44
2	0.00	24.30	6.00	11.10	15.81	5.68

Table 2: Statistics related to the velocity components

Trial	Min	Max	Q_1	Median	Q_2	Std Dev
			$V_x(x)$ (m/s)			
1	-0.2339	0.2857	-0.0325	-0.0004	0.0311	0.0495
2	-0.2769	0.2851	-0.0294	0.0000	0.0304	0.0506
			$V_z(z)$ (m/s)			
1	0.3231	0.2395	-0.0317	-0.0008	0.0333	0.0513
2	-0.3894	0.4188	-0.0309	-0.0008	0.0315	0.0549
			$V_y(y)$ (m/s)			
1	-0.2105	0.1584	-0.0184	-0.0025	0.0103	0.0214
2	-0.2762	0.1682	-0.0212	-0.0031	0.0112	0.0250

The frequency distributions of the horizontal coordinates x and z and of the corresponding velocity components seem to follow a symetric normal distribution. The particle's behaviour with respect to x and z is the same, as shown by the statistical indicators. The width of the x values (21.8 and 22.1 mm) is slightly smaller than the inner diameter of the test tube (24 mm). The higher width of the z values (24.6 and 23.71 mm) are likely due to the higher values of the random errors (see appendix, Figure A.3). The frequency distribution of y is characterised by an increase, a

plateau and a steep decrease at the highest heights. The largest measured height (24.30 mm) represents only 16.2% of the total height of the test tube (150 mm) and 4.05 times the height of the powder bed (6 mm). This means that the particle considered here (whose diameters are between 80 μm and 150 μm) are apparently too large and heavy for reaching the height where they could exit the test tube over the duration of the experiment. The frequency distribution of the vertical velocity V_y is non-symetrical and biased towards negative values. This can be plausibly attributed to the effect of gravity and the smaller numbers of collisions with other aerosols as shall be seen later.

In Figure 9 and in Table 3, the features of the velocity and the kinetic energy are shown.

Table 3: Statistics related to pV

Trial	Min	Max	Q_1	Median	Q_2	Std Dev
			V (m/s)			
1	0.0024	0.3491	0.0385	0.0615	0.0854	0.0366
2	0.0052	0.4477	0.0355	0.0611	0.0883	0.0422
Average			**0.0370**	**0.0613**	**0.0869**	**0.0394**
			$E.10^{11}$ (J)			
1	0.0012	27.3551	0.3326	0.8490	1.6382	1.7089
2	0.0061	44.9969	0.2822	0.8374	1.7511	2.3108
Average			**0.3074**	**0.8432**	**1.6947**	**2.0099**

The kinetic energy distribution follows a decreasing exponential shape. The frequency distribution of the velocity V is assymetrical and is characterised by a smooth increase followed by a steep decrease in both cases. To explore the cause of this, we represented the *average* values of the velocity (and velocity components) as a function of the horizontal coordinate x and the vertical coordinate y in Figure 10. We show the results of the repeated trials in the appendix (see Figures A.7 - A.8). The largest values of the velocity $\bar{V}$ are found at the highest heights where the highest descending values of $\bar{V_y}$ are also seen. This indicates that these highest velocities might stem from the effects of gravity on the particle. As function of the horizontal coordinate x, the highest velocity values are found near the wall of the test tube. It is worth noting that $\bar{V_y}(x)$ points upwards at the middle of the test tube but downards when x approaches the extremity of the test tube. In Figure 11, all points where the particle goes upwards and downwards are represented with respect to the horizontal coordinates x and z. It can be seen that the particle rarely moves downward around the middle of the test tube. On the other hand, the particle also seldom moves upward near the

wall of the test tube. The region where the upward and downward motions overlap is narrow. It is noteworthy that the highest values of the average velocity $\bar{V}$ are found in regions where the presence frequency of the particle is the lowest (highest heights and areas close to the inner wall). Besides the gravity, the higher values of the velocity might stem from a decrease in the number of shocks due to lower population densities.

In Figure 12, the local circulation (from $t = 200$ s to $t = 207$ s) and the average circulation (over the whole steady state, i.e. between $t = 20$ s and $t = 700$ s) have been represented. On average, the particle tends to move upward with a low velocity around the middle of the test tube whereas it falls back at a much higher speed beside the inner wall of the test tube. The time-averaged velocities are considerably smaller in the horizontal middle of the test tube. The local values are much less regular.

5. Conclusions and outlook

In this work, we wanted to develop a methodology allowing us to study the behaviour of detached aerosol particles in a test tube agitated by a vortex shaker and apply it to our standard conditions, as such data are necessary for understanding dust emission and developping predictive models.

In Section 2, we describe PEPT and the vortex shaker. In Section 3, we describe and validate the statistical methods we used. Giving the short-range motion of the particle and the small dimension of the test tube, averaging and smoothing did not prove to be good strategies for computing a physically realistic velocity. Instead, a filtering approach was adopted, in that only a motion covering at least a critical distance d_{crit} is considered.

Based on this, we assessed the particle's behaviour under standard conditions, that is at a rotation speed of 1500 rpm while an air flow goes through the open test tube filled with 2 g of powder. We considered $CaCO_3$ powder whose aerodynamic diameters are between 80μ m and 150μ m. Since we could not radio-activate its particles, we used a tracer particle of alumina with similar physical characteristics instead. The local instantaneous trajectory of the particle has a chaotic aspect which makes it hard to identify any trends apart from the circular nature of the motion. A statistical treatment of the measured positions and filtered velocities allows one, however, to identify important features of the macroscopic behaviour of the particle. The frequency distributions of the horizontal coordinates x and z and of the corresponding velocity components V_x and V_z follow approximately a Gaussian shape. The frequency distribution of the height y is characterised by a strong increase, an even stronger decrease and a plateau between $y =$ 5 mm and $y = 20$ mm. The heights reached by the particle are much inferior to the height of the test tube (150 mm).

The highest values of the velocity are found at the highest heights and close to the inner wall of the test tube, where the population densities are thinner.

The data we obtained in the present study are the first step for establishing numerical models building a bridge between theory and experiments, which is in itself one of the main goals of powder technology [48]. A combination of CFD (Eulerian - Lagrangian) and DEM (Direct Element Modelling) seems to be a promising way to develop predictive models [49]. Wangchai et al. [50] investigated the particle flow mechanisms of powders within a rotating drum dustiness tester through a combination of experimental work and DEM. They found out that while useful, DEM cannot capture all the flow patterns in a dustiness tester which are crucial for understanding the bevahiour of the produced aerosols. CFD appears to be a good complementary approach to reaching a truly holistic view of the phenomena underlying dust generation. We intend to use the data of this study as a basis for simulating the motion of the particles within the agitated test tube. This, in turn, shall allow us to model the whole aerosolisation process, including the movement of the particles in the bulk, the interaction between particles and the formation of the first aerosols.

Our study opens up another research endeavour that is worth mentioning. Kahrizsangi et al. [51, 52] conducted a parametric study of dustiness within a fludised bed vibrating with different frequencies and accelerations. While they could well account for the effects stemming from changes in the acceleration, they were not able to provide an intuitive physical explanation of the bearing of the frequency on dustiness. We intend to perform a similar parametric study of our system relying on PEPT which will concern the most important variables, i.e. the mass, the rotation speed and the size of the tracer particle.

6. Acknowledgements

We acknowledge Dr. Thomas Leadbeater (who worked previously at the University of Birmingham in the UK) for preparing the activated alumina tracer particle for the experiments at the University of Birmingham. We would also like to acknowledge Prof. J.P.K. Seville (University of Surrey, UK) for his useful insights regarding the use of PEPT for this study. This work was supported by the European Union FP7 Marie Curie Actions Initial Training Network T-MAPPP (Training in Multiscale Analysis of MultiPhase Particulate Processes and Systems) under grant agreement No 607453 and the Region Picardie/ Hauts de France and by the Programme 190 (French Ministry of Environment). We solemny declare that there are no conflicts of interest.

References

[1] E. Petavratzi, S. Kingman, I. Lowndes, Particulates from mining operations: A review of sources, effects and regulations, Minerals Engineering 18 (2005) 1183–1199.

[2] D. Dahmann, C. Monz, Determination of dustiness of nanostructured materials, Gefahrstoffe - Reinhaltung der Luft 71 (2011) 481–487.

[3] I. Ogura, H. Sakurai, M. Gamo, Dustiness testing of engineered nanomaterials, Journal of Physics: Conference Series 170 (2009) 012003.

[4] A. Klippel, M. Schmidt, U. Krause, Dustiness in workplace safety and explosion protection–review and outlook, Journal of Loss Prevention in the Process Industries 34 (2015) 22–29.

[5] D. E. Evans, L. A. Turkevich, T. Roettgers, G. J. Deye, P. A. Baron, Dustiness of Fine and Nanoscale Powders, Annals of Occupational Hygiene 57 (2013) 261–277.

[6] A. Maynard, P. Baron, M. Foley, Exposure to carbon nanotube material: aerosol release during the handling of unrefined single-walled carbon nanotube material, Journal of Toxicology (2004).

[7] A. D. Maynard, E. D. Kuempel, Airborne nanostructured particles and occupational health, Journal of Nanoparticle Research 7 (2005) 587–614.

[8] O. L. C. Le Bihan, A. Ustache, D. Bernard, O. Aguerre-Chariol, M. Morgeneyer, Experimental study of the aerosolization from a carbon nanotube bulk by a vortex shaker, Journal of Nanomaterials 2014 (2014) 7.

[9] Y. Ding, B. Stahlmecke, H. Kaminski, Y. Jiang, T. A. Kuhlbusch, M. Riediker, Deagglomeration testing of airborne nanoparticle agglomerates: Stability analysis under varied aerodynamic shear and relative humidity conditions, Aerosol Science and Technology 50 (2016) 1253–1263.

[10] S. Kamath, V. Puri, H. Manbeck, R. Hogg, Flow properties of powders using four testersmeasurement, comparison and assessment, Powder technology 76 (1993) 277–289.

[11] W. A. Heitbrink, W. F. Todd, T. C. Cooper, D. M. O'Brien, The application of dustiness tests to the prediction of worker dust exposure, The American Industrial Hygiene Association Journal 51 (1990) 217–223.

[12] S. Bach, U. Eickmann, E. Schmidt, Comparison of established systems for measuring the dustiness of powders with the unc dustiness tester developed especially for pharmaceutical substances, Annals of occupational hygiene (2013) met022.

[13] F. Hamelmann, E. Schmidt, Methods of estimating the dustiness of industrial powders–a review, KONA Powder and Particle Journal 21 (2003) 7–18.

[14] M. A. Plinke, R. Maus, D. Leith, Experimental examination of factors that affect dust generation by using heubach and mri testers, The American Industrial Hygiene Association Journal 53 (1992) 325–330.

[15] C. EN 15051, 15051 workplace atmospheresmeasurement of the dustiness of bulk materialsrequirements and test methods, Brussels, Belgium: European committee for standardization (2006).

[16] M. Boundy, D. Leith, T. Polton, Method to evaluate the dustiness of pharmaceutical powders, Annals of Occupational Hygiene 50 (2006) 453–458.

[17] M. Morgeneyer, O. Le Bihan, A. Ustache, O. Aguerre-Chariol, Experimental study of the aerosolization of fine alumina particles from bulk by a vortex shaker, Powder Technology 246 (2013) 583–589.

[18] S. Chakravarty, O. Le Bihan, M. Fischer, M. Morgeneyer, Dust generation in powders: Effect of particle size distribution, in: EPJ Web of Conferences, volume 140, EDP Sciences, p. 13018.

[19] F. Durst, A. Melling, J. H. Whitelaw, Principles and practice of laser-doppler anemometry, NASA STI/Recon Technical Report A 76 (1976).

[20] R. J. Adrian, J. Westerweel, Particle image velocimetry, 30, Cambridge University Press, 2011.

[21] J. G. Santiago, S. T. Wereley, C. D. Meinhart, D. Beebe, R. J. Adrian, A particle image velocimetry system for microfluidics, Experiments in fluids 25 (1998) 316–319.

[22] C. Willert, Stereoscopic digital particle image velocimetry for application in wind tunnel flows, Measurement science and technology 8 (1997) 1465.

[23] I. Nezu, W. Rodi, Open-channel flow measurements with a laser doppler anemometer, Journal of Hydraulic Engineering 112 (1986) 335–355.

[24] A. P. Yoganathan, W. H. Corcoran, E. C. Harrison, In vitro velocity measurements in the vicinity of aortic prostheses, Journal of biomechanics 12 (1979) 135–152.

[25] A. Ochieng, M. Onyango, K. Kiriamiti, Experimental measurement and computational fluid dynamics simulation of mixing in a stirred tank: a review, South African Journal of Science 105 (2009) 421–426.

[26] Z.-C. Liu, C. Landreth, R. Adrian, T. Hanratty, High resolution measurement of turbulent structure in a channel with particle image velocimetry, Experiments in fluids 10 (1991) 301–312.

[27] R. Ettema, I. Fujita, M. Muste, A. Kruger, Particle-image velocimetry for whole-field measurement of ice velocities, Cold Regions Science and Technology 26 (1997) 97–112.

[28] B. Guo, D. F. Fletcher, T. A. Langrish, Simulation of the agglomeration in a spray using lagrangian particle tracking, Applied Mathematical Modelling 28 (2004) 273–290.

[29] P. W. Longest, J. Xi, Effectiveness of direct lagrangian tracking models for simulating nanoparticle deposition in the upper airways, Aerosol Science and Technology 41 (2007) 380–397.

[30] J. Seville, A Single Particle View Of Fluidization, The 13th International Conference on Fluidization - New Paradigm in Fluidization Engineering, 2010, pp. 1–11.

[31] J. Chaouki, F. Larachi, M. Dudukovic, Non-invasive monitoring of multiphase flows, Elsevier, 1997.

[32] J. A. Laverman, I. Roghair, M. v. S. Annaland, H. Kuipers, Investigation into the hydrodynamics of gas–solid fluidized beds using particle image velocimetry coupled with digital image analysis, The Canadian Journal of Chemical Engineering 86 (2008) 523–535.

[33] R. Ansart, P. Garcia-Trinanes, B. Boissiere, H. Benoit, J. Seville, O. Simonin, Dense gas-particle suspension upward flow used as heat transfer fluid in solar receiver: Pept experiments and 3d numerical simulations, Powder Technology 307 (2017) 126–137.

[34] D. Parker, A. Dijkstra, I. Martin, J. P. K. Seville, Positron emission particle tracking studies of spherical particle motion in rotating drums, Chemical Engineering Science 52 (1997) 2011–2022.

[35] T. Volkwyn, A. Buffler, I. Govender, J.-P. Franzidis, A. Morrison, A. Odo, N. Van Der Meulen, C. Vermeulen, Studies of the effect of tracer activity on time-averaged positron emission particle tracking measurements on tumbling mills at pept cape town, Minerals Engineering 24 (2011) 261–266.

[36] M. Stein, Y. Ding, J. Seville, Experimental verification of the scaling relationships for bubbling gas-fluidised beds using the pept technique, Chemical Engineering Science 57 (2002) 3649–3658.

[37] D. J. Parker, C. J. Broadbent, P. Fowles, M. R. Hawkesworth, Positron emission particle tracking-a technique for studying flow within engineering equipment, Nuclear Instruments and Methods in Physics Research Section A: Accelerators, Spectrometers, Detectors and Associated Equipment 326 (1993) 592–607.

[38] M. Tan, D. Parker, P. Dee, Pept data presentation software, manual, Birmingham University, UK (1997).

[39] J. Seville, A. Ingram, X. Fan, D. Parker, Positron emission imaging in chemical engineering, Advances in Chemical Engineering 37 (2009) 149–178.

[40] D. Valdesueiro, P. Garcia-Triñanes, G. Meesters, M. Kreutzer, J. Gargiuli, T. Leadbeater, D. Parker, J. Seville, J. van Ommen, Enhancing the activation of silicon carbide tracer particles for pept applications using gas-phase deposition of alumina at room temperature and atmospheric pressure, Nuclear Instruments and Methods in Physics Research Section A: Accelerators, Spectrometers, Detectors and Associated Equipment 807 (2016) 108–113.

[41] D. Parker, R. Forster, P. Fowles, P. Takhar, Positron emission particle tracking using the new birmingham positron camera, Nuclear Instruments and Methods in Physics Research Section A: Accelerators, Spectrometers, Detectors and Associated Equipment 477 (2002) 540–545.

[42] M. Van de Velden, J. Baeyens, J. P. K. Seville, X. Fan, The solids flow in the riser of a Circulating Fluidised Bed (CFB) viewed by Positron Emission Particle Tracking (PEPT), Powder Technology 183 (2008) 290–296.

[43] M. Marigo, M. Davies, T. Leadbeater, D. L. Cairns, A. Ingram, E. H. Stitt, Application of Positron Emission Particle Tracking (PEPT) to validate a Discrete Element Method (DEM) model of granular flow and mixing in the Turbula mixer, International journal of pharmaceutics 446 (2013) 46–58.

[44] D. J. Parker, X. Fan, Positron emission particle trackingapplication and labelling techniques, Particuology 6 (2008) 16–23.

[45] D. Parker, P. McNeil, Positron emission tomography for process applications, Measurement Science and Technology 7 (1996) 287.

[46] H. Shi, R. Mohanty, S. Chakravarty, R. Cabiscol, M. Morgeneyer, H. Zetzener, J. Ooi, A. Kwade, S. Luding, V. Magnanimo, Effect of particle size and cohesion on powders yielding and flow, KONA Powder and particle journal, accepted for the publication (2017).

[47] W. H. Press, S. A. Teukolsky, W. T. Vetterling, B. P. Flannery, Numerical Recipes in C (2Nd Ed.): The Art of Scientific Computing, Cambridge University Press, New York, NY, USA, 1992.

[48] I. Tomasetta, D. Barletta, M. Poletto, Correlation of powder flow properties to interparticle interactions at ambient and high temperatures, Particuology 12 (2014) 90–99.

[49] L. E. Stone, P. W. Wypych, D. B. Hastie, S. Zigan, et al., Cfd-dem modelling of powder flows and dust generation mechanisms-a review, in: 12th International Conference on Bulk Materials Storage, Handling and Transportation (ICBMH 2016), The, Engineers Australia, p. 417.

[50] S. Wangchai, D. B. Hastie, P. W. Wypych, The investigation of particle flow mechanisms of bulk materials in dustiness testers, Particulate Science and Technology 34 (2016) 241–254.

[51] H. S. Kahrizsangi, D. Sofia, D. Barletta, M. Poletto, Dust generation in vibrated cohesive powders, CHEMICAL ENGINEERING 43 (2015) 769–774.

[52] D. Barletta, P. Russo, M. Poletto, Dynamic response of a vibrated fluidized bed of fine and cohesive powders, Powder technology 237 (2013) 276–285.

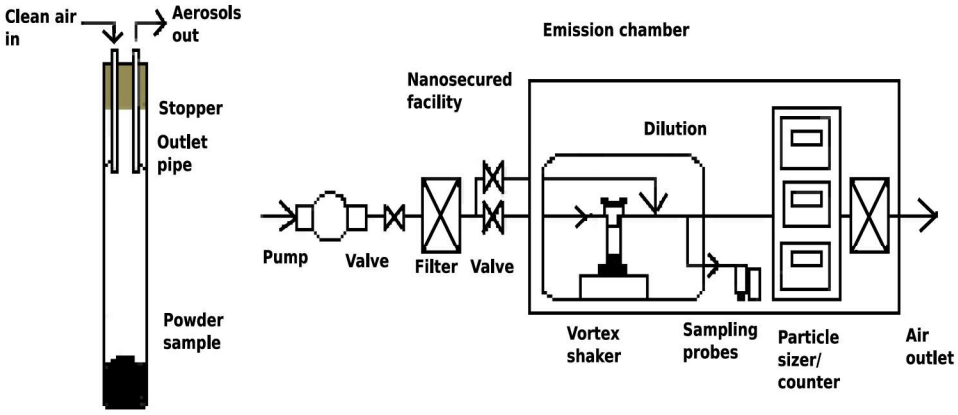

Figure 1: The vortex shaker experiment [17]

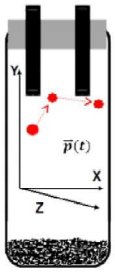

Figure 2: Axes within the Test Tube

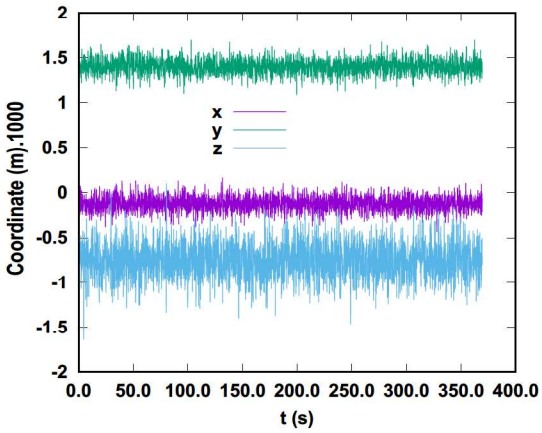

Figure 3: Measured position in a closed non-agitated vortex-shaker

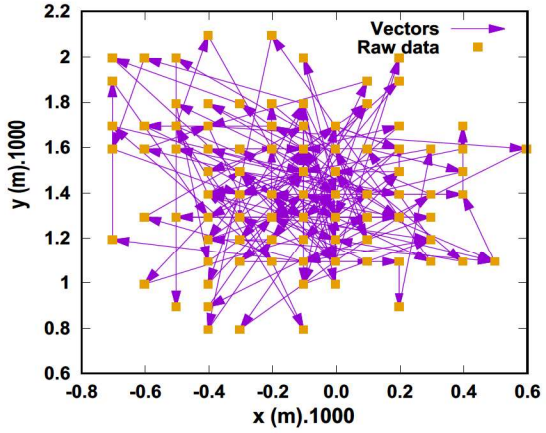

(a) Non-Filtered vectors

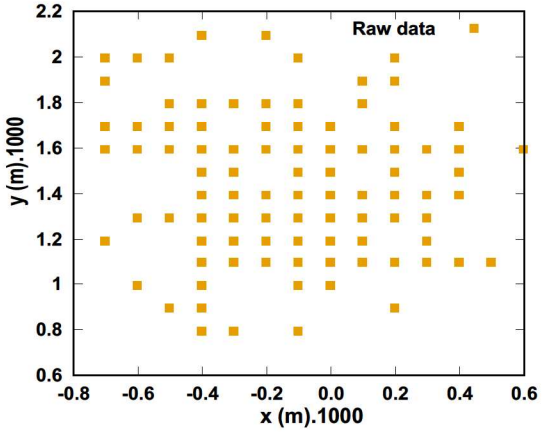

(b) Filtered vectors

Figure 5: Pseudo-trajectory for the stationary trial. Lenght units are in mm.

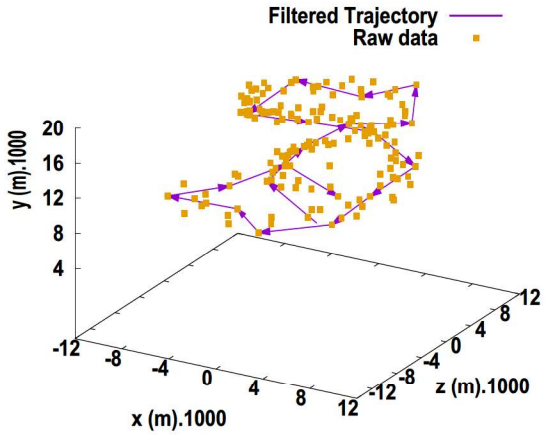

(a) Filtered trajectory

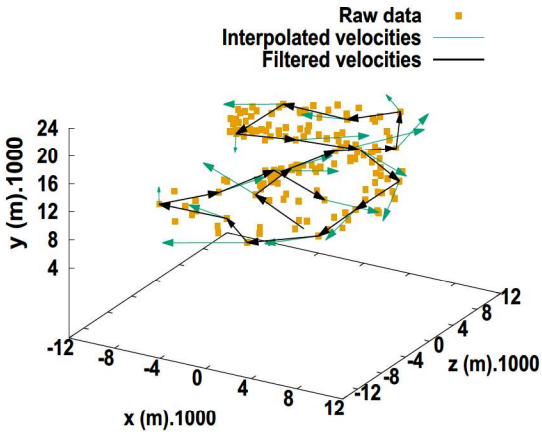

(b) Smoothed trajectory with 10 neighbouring points

Figure 6: Filterig and smoothing for $\omega = 1500$ rpm, close test tube and $t \subset [100 : 102, 0]$ s. Lenght units are in mm.

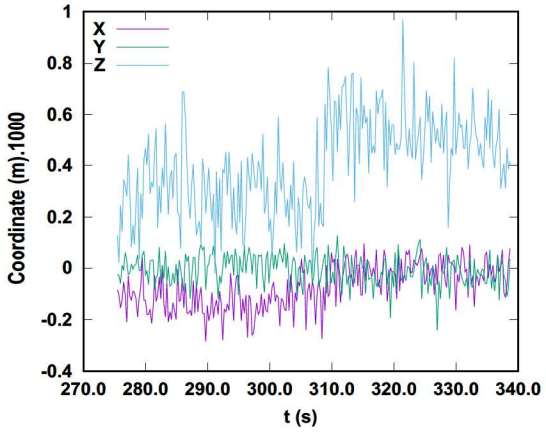

(a) 20 time points

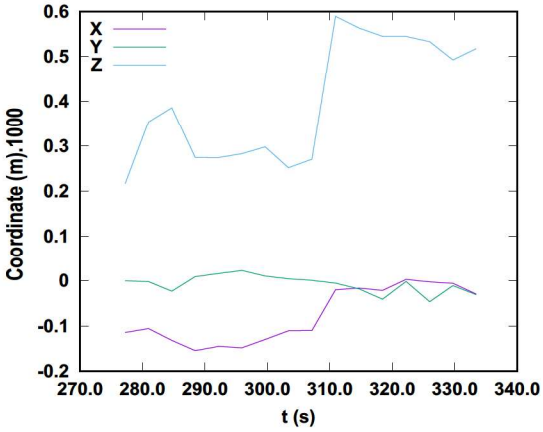

(b) 50 time points

Figure 4: Locally averaged coordinates. Lenght units are in mm.

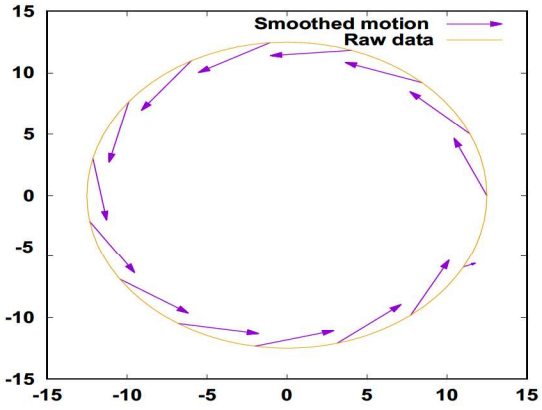

(a) Smoothing with ten neighbouring points

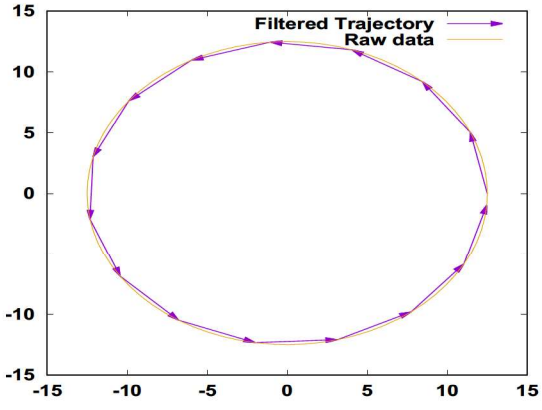

(b) Filtering

Figure 7: Smoothing and filtering of a circular movement (units: mm)

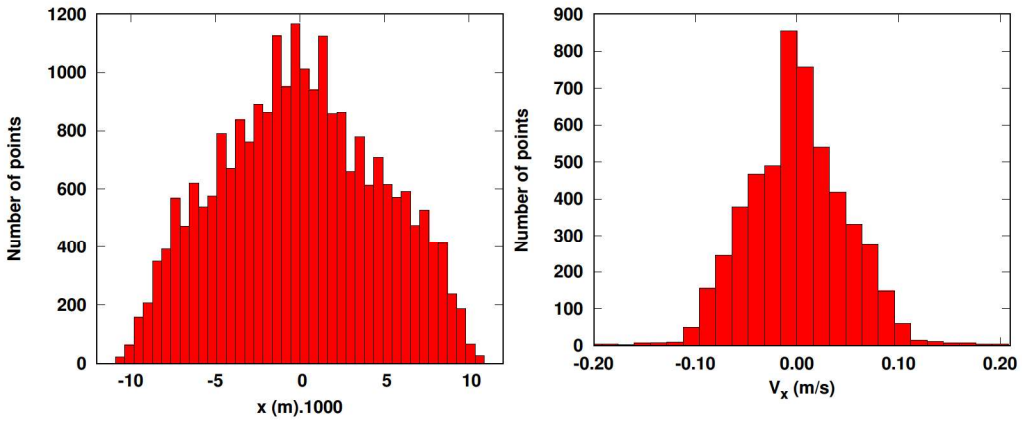

(a) Distribution of x (b) Distribution of V_x

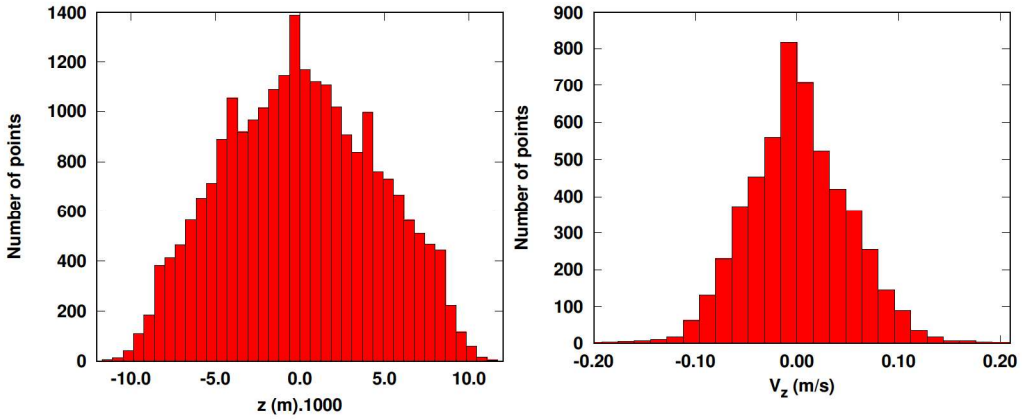

(c) Distribution of z (d) Distribution of V_z

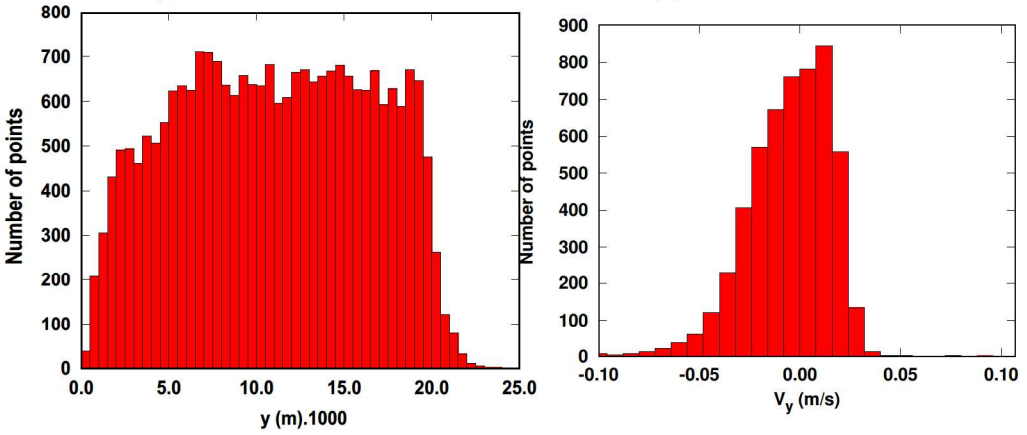

(e) Distribution of y (f) Distribution of V_y

Figure 8: Distribution of the coordinates and velocity components. Lenght units are in mm.

Figure 9: Frequency distribution of the velocity and kinetic energy

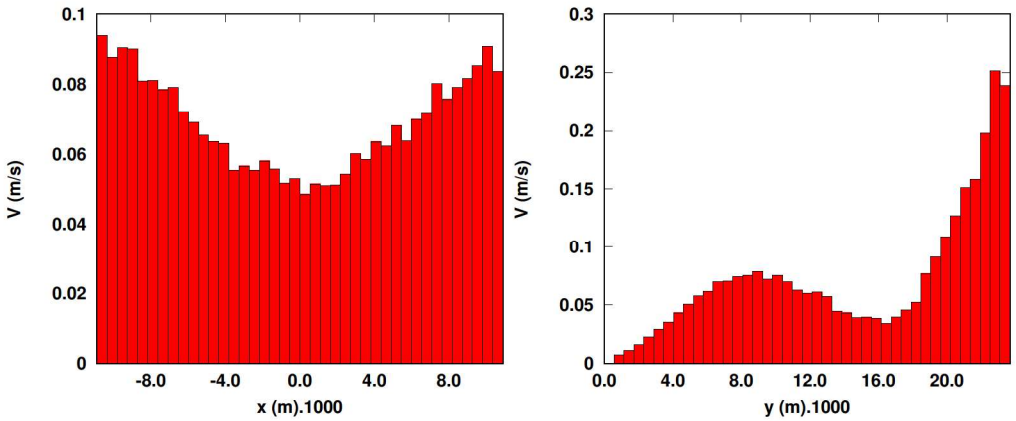

(a) $V\bar{(}x)$, first trial (b) $V\bar{(}y)$, second trial

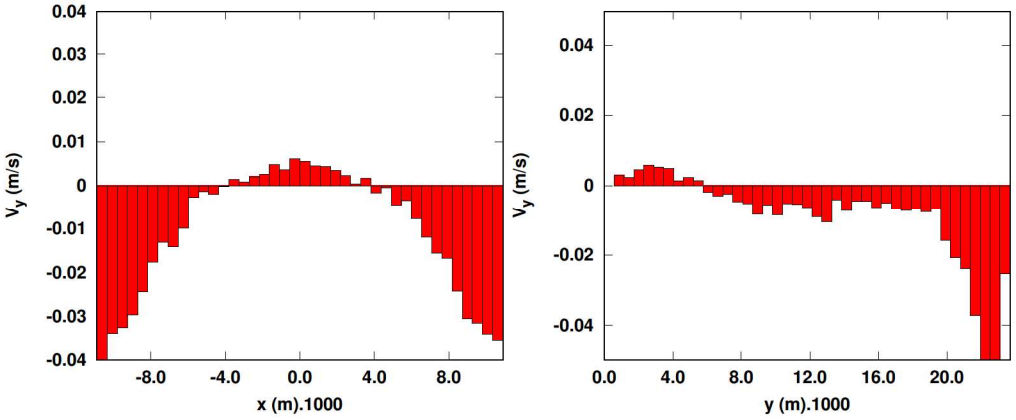

(c) $V_y\bar{(}x)$, first trial (d) $V_y\bar{(}y)$, second trial

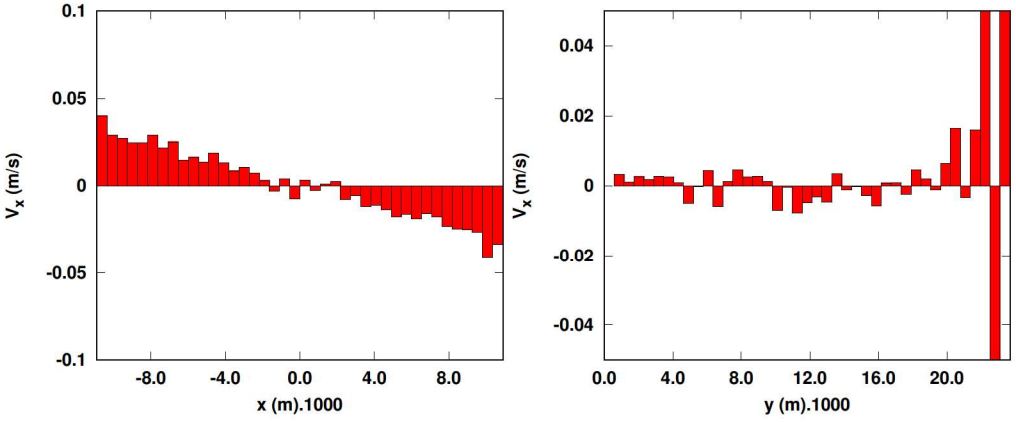

(e) $V_x\bar{(}x)$ (f) $V_x\bar{(}y)$

Figure 10: Time-averaged velocity as a function of x and y. Lenght units are in mm.

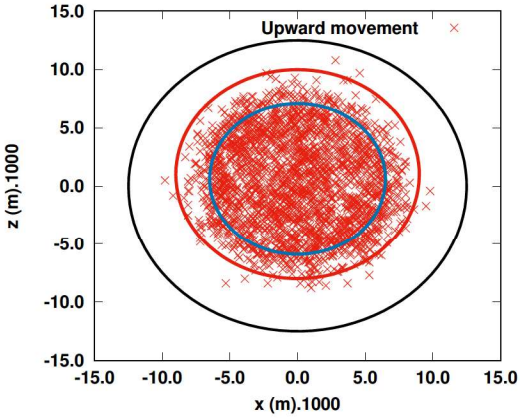

(a) Upward movement

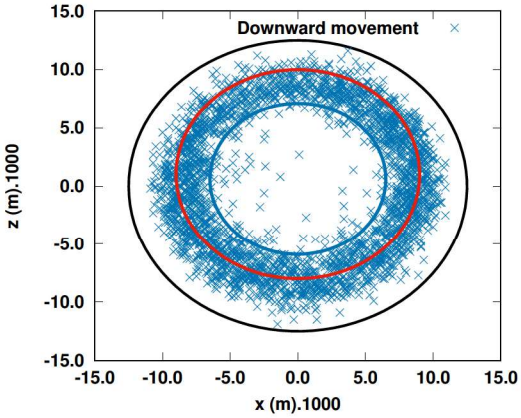

(b) Downward movement

Figure 11: Distribution of the upward and downward movement. Large circle: inner wall. Small circles: imaginary boundaries of the upward and downward movements

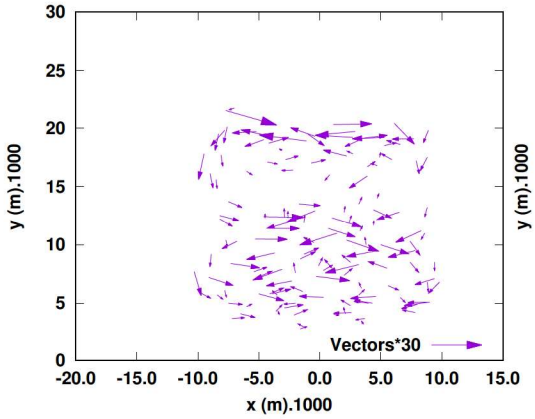

(a) Local vectors with respect to x and y

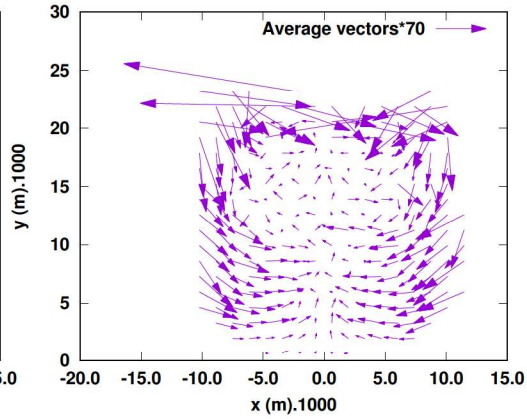

(b) Average vectors with respect to x and y

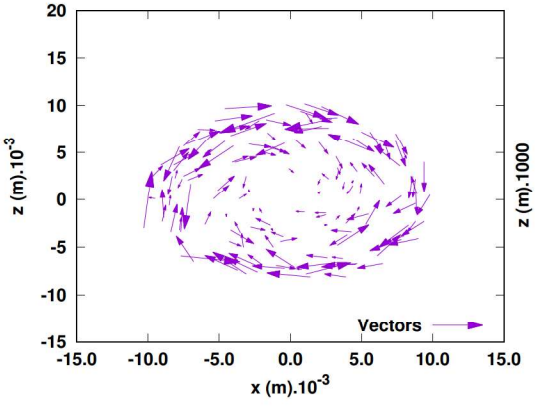

(c) Local vectors with respect to x and z

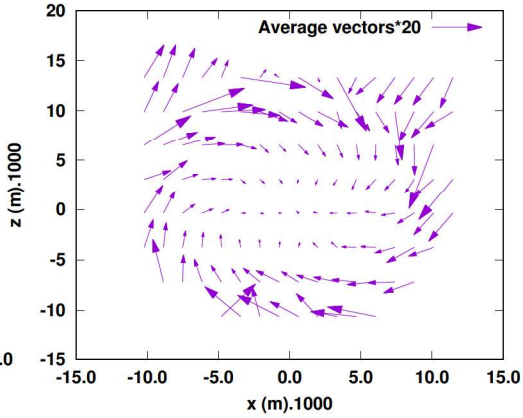

(d) Average vectors with respect to x and z

Figure 12: Local instantaneous ([200.00; 217.00] s) and time-averaged velocity vectors. Lenght units are in mm.